

RSC Advances



This is an *Accepted Manuscript*, which has been through the Royal Society of Chemistry peer review process and has been accepted for publication.

Accepted Manuscripts are published online shortly after acceptance, before technical editing, formatting and proof reading. Using this free service, authors can make their results available to the community, in citable form, before we publish the edited article. This *Accepted Manuscript* will be replaced by the edited, formatted and paginated article as soon as this is available.

You can find more information about *Accepted Manuscripts* in the [Information for Authors](#).

Please note that technical editing may introduce minor changes to the text and/or graphics, which may alter content. The journal's standard [Terms & Conditions](#) and the [Ethical guidelines](#) still apply. In no event shall the Royal Society of Chemistry be held responsible for any errors or omissions in this *Accepted Manuscript* or any consequences arising from the use of any information it contains.

ARTICLE

Synthesis and structure of free-standing germanium quantum dots and their application in live cell imaging

Cite this: DOI: 10.1039/x0xx00000x

Received 00th January 2012,

Accepted 00th January 2012

DOI: 10.1039/x0xx00000x

www.rsc.org/

Ali Karatutlu*,^{a,f} Mingying Song,^a Ann P. Wheeler,^b Osman Ersoy,^a William R. Little,^a Yuanpeng Zhang,^a Pascal Puech,^c Filippo S. Boi,^d Zofia Luklinska^e and Andrei V. Sapelkin^a

Free-standing Ge quantum dots around 3 nm in size were synthesized using a bench-top colloidal method and suspended in water and ethanol. In the ethanol solution, the photoluminescence of the Ge quantum dots was observed between 650 and 800 nm. Structural and optical properties of these colloidal Ge quantum dots were investigated by utilizing X-ray diffraction, X-ray absorption spectroscopy, Raman spectroscopy, and photoluminescence spectroscopy and transmission electron microscopy. The structure of as-prepared Ge quantum dots that was found is best described by a core/shell model with a small crystalline core and an amorphous outer shell with a surface that was terminated by hydrogen-related species. As-prepared Ge quantum dots were suspended in cell growth medium, and then loaded into Cervical Carcinoma (HeLa) cells. The fluorescent microscopy images were then collected using 405 nm, 488 nm, 561 nm and 647 nm wavelengths. We observed that, based on fluorescence measurements, as-prepared Ge quantum dots can remain stable for up to 4 weeks in water. Investigation of toxicity, based on a viability test, of as-prepared uncoated Ge quantum dots in the HeLa cells was carried out and compared with the commercial carboxyl coated CdSe/ZnSe quantum dots. The viability tests show that Ge quantum dots are less toxic when compared to commercial carboxyl coated CdSe/ZnS quantum dots.

Introduction

Real time monitoring of a cell's function and state can be carried out by using visible and near-infrared emitting luminescent nano-scale particles, which are also known as quantum dots (Qdots)^{1,2}. The repetition and reliability of the luminescence at room temperature from various inorganic qdots make them excellent candidates for the detection of biomolecular interplay and imaging applications in vivo²⁻⁶. Qdots also have a high resistivity to photobleaching and their narrow emission and broad absorption bands can be tuned by varying the particle size and composition. Thus, quantum yield, small size and lack of photobleaching are some of the reasons why qdots are becoming a popular alternative to fluorescent organic dyes for biological fluorescent imaging^{4,7}. CdSe/ZnS-based qdots currently hold the dominant position in bio-imaging applications. However, CdX (X=Se, Te) qdots show significant levels of cytotoxicity when used in cell imaging/diagnostics^{8,9}. When CdSe has been coated with ZnS there is still a considerable cytotoxic effect¹⁰. At the end of 24 hours, approximately 40 % of the macrophage cells was observed as killed even with small concentrations of CdSe/ZnS qdots (e.g. 2.5 nM).

An alternative system is the InP qdots, however, production of high quality qdots is more challenging for these materials than for the Cd-based systems³. Group 4 materials (C, Si and Ge) can offer a viable alternative due to relatively low toxicity^{6,11,12}. Their optical properties can also be radically enhanced by exploiting the quantum confinement effect (QCE)¹³⁻¹⁶. Ge qdots are expected to show these unique properties in accordance with the QCE for relatively large particles due to the fact that its exciton Bohr radius is estimated to be larger ($R_B=24.3$ nm) than that of Si ($R_B = 4.9$ nm)¹⁷. One of the fundamental problems that preclude the wider use of Si and Ge in imaging application is an indirect band gap that results in a relatively inefficient light emission. However, this can be improved by the QCE as has originally been demonstrated for porous Si by L. Canham in 1991^{13,14}. Modifying the surface species can also alter the optical properties of these qdots and can improve their stability by saturating the dangling bonds for instance by hydrogen or carbon atoms^{18,19}. For over 20 years various physical and chemical routes of the synthesis of Ge qdots have been reported^{15,20,21,17,22-29}. A novel and significant method of colloidal synthesis, particularly reducing the halides (GeI₂/GeI₄), was recently reported as the most elegant method in

terms of size/shape modification and the stability of Ge qdots^{28–30}. However, this method requires the high temperature Schlenk technique which makes it rather elaborate. Recently, colloidal synthesis methods^[26,30] have become available using room temperature benchtop chemistry. These methods seem to yield small Ge qdots and allow for some control over size selectivity as well. However, potential suitability of these Ge qdots for bio-applications would significantly depend on their atomic structure, morphology and surface termination as each of these physiochemical properties are essential to understand the toxicity of qdots³¹. For example, oxygen-terminated Ge qdots may have limited use in bio-application due to water solubility of germanium oxide. It has been suggested²⁶ that, following the benchtop colloidal synthesis, the structure of as-prepared Ge qdots is amorphous (based on the X-ray diffraction), while the sample seems to be crystalline according to the selective area electron diffraction (SAED) results²⁷. The latter may suggest a transformation to a crystalline phase due to annealing in the highly energetic electron beams used in TEM. The nature and stability of the surface is also unclear. Furthermore, there are some reports suggesting a Ge tetragonal phase (ST-12 phase) may be obtained upon deposition by the cluster beam evaporation technique^{32,33}, releasing of high pressure³⁴ or annealing at high temperature. There are also some studies including lithiation³⁵ and aging³⁶ that show ST-12 phases mixed together either with lithium atoms or the diamond cubic phase of Ge. The ST-12 phase has a potential for opto-electronic applications since it is predicted to be a direct band gap material ($E_g=1.47$ eV)³⁷.

Despite the potential in the biomedical applications of Ge qdots there are few studies on biological imaging and the toxicity of Ge qdots^{38,39}. Herein we present a slightly modified method of the preparation of Ge qdots to yield colloiddally stable Ge qdots. We use a combination of direct visual techniques, such as TEM, together with short range (X-ray absorption spectroscopy, Raman) and long range (XRD, Raman) sensitive structural methods to investigate atomic arrangements on the sub-nanoscale. We test biocompatibility of Ge qdots using the viability test and compare it with the commercial carboxyl coated CdSe/ZnS qdots. We also assess the potential of Ge qdots for cell imaging applications.

Experimental

Materials and methods

Materials

The chemicals, GeCl_4 (>99%), ethylene glycol (ETG, 99%), and 2 M of sodium borohydride solution in triethylene glycol dimethyl ether ('the triglyme') were used as purchased from Sigma-Aldrich. Polyvinylpyrrolidone (PVP) (MW=630,000) were used as purchased from Tokyo-chemicals.

Synthesis of Ge qdots

Ge qdots, named as CS_1 , were synthesized by a slight modification of a benchtop *colloidal synthesis* route²⁷ which produces CS_1 suspended in water and ethanol. In the first part of the synthesis 265 μL of GeCl_4 were reduced using a solution of 10 mL of ETG and 50 mg of PVP. 6 mL of the triglyme was then added at a rate of 90 ml/hour for the first 2 ml and then 9 ml/hour for the remaining 4 ml. This controlled addition process of the triglyme was performed with a syringe pump into a 3 neck round bottom beaker in which the solution was bubbled using a continuous Ar gas flow with an inlet of a micro-tube through

the solution. The formation process took approximately 1 hour and the final product was separated from the colloidal chemical solution by 10 minutes of centrifugation at 10,000 rpm.

Characterization of Ge qdots

After the synthesis, Raman spectroscopy and photoluminescence (PL) spectroscopy measurements were conducted with a Renishaw 1000 spectrometer. A diode laser at a wavelength of 473 nm was used for CS_1 , whereas for the Ge-H stretching mode of CS_1 , a He-Ne laser at a wavelength of 633 nm was used. TEM measurements were taken using a JEOL 2010 to characterize the morphology and the size of CS_1 . Gatan digital micrograph software was used for the size analysis by TEM. XRD and EXAFS measurements were conducted in the beamline B18⁴⁰ at Diamond Light Source in the UK. The EXAFS measurement was carried out at $T=100$ K using a cryojet system. ATHENA⁴¹ was used to extract the absorption spectrum from the raw data. Then, the structural parameters were determined using the least squared fit of the EXAFS data in r -space with ARTEMIS⁴¹ by FEFF6 code⁴² within the fitting range of the photoelectron momentum (k) and the non-phase corrected radial distribution distance (r) of 3–16 \AA^{-1} and 1.67–2.55 \AA respectively. Energy resolution of EXAFS experiment was 1 eV.

Cell Culture

The Cervical Carcinoma cells (HeLa cells) were cultured in a growth medium (89% high glucose DMEM, 10 % Foetal Calf Serum, 1 % Penicillin & Streptomycin) with various densities inside 6-well plates according to the following trials. Cells were split once a week and incubated in a 5% CO_2 atmosphere at 37 $^\circ\text{C}$. In the fixation steps, cells were firstly washed 2 times with Phosphate Buffered Saline solution (PBS), and incubated with 2 mL of 4 % Paraformaldehyde solution (PFA) per well for 10 minutes at room temperature, followed by washing 3 times with PBS. Fixed cells dishes or plates were then stored in a fridge for 24 hours before post procedures.

Visualization of Ge qdots in HeLa Cells

In order to investigate the Ge qdots impacts on HeLa cells, sample of HeLa cells with Ge qdots were prepared and imaged. HeLa cells were seeded on a glass coverslip in a 6-well plate at a density of 5.0×10^3 cells ml^{-1} well⁻¹, incubated overnight with 50 nmole of Ge qdots per well. Ge qdots were synthesized, suspended in water and sterilized under UV light for 15 minutes. Ge qdots were re-suspended in growth medium. Ge qdots with different concentrations suspended in growth medium were loaded to the HeLa cells. The cells were fixed with PFA prior to fluorescence imaging.

Fluorescence images were acquired on a spinning disk confocal microscopy (consisting of a Nikon ECLIPSE TE2000-s microscope, a YOKOGAWA CSU-x1 spinning disk, and a 100X objective, NA 1.4). Sample was excited with four different wavelength lasers (405 nm, 488 nm, 561 nm and 640 nm). Images were captured using an Andor-iXon3 885 camera and data were post processed on ImageJ.

The incoming laser was modulated through an acousto-optical tunable filter (AOTF) before being recorded by CCD camera. The reflected light from a mirror sample slide were recorded using an optical power meter (Newport 1916-C).

Cell Viability Test

Once the optical stability of Ge qdots (CS₁) in cells was confirmed the toxicity test was performed. Series of viability test were taken and each test were repeated 3 times.

To examine the toxicity, fresh CS₁ samples were produced and tested on HeLa cells. HeLa cells were cultivated as described in section 2.3. Cells were seeded into a 12-well plate at a density of 5.0×10^3 cells ml⁻¹ well⁻¹. Ge qdots were added into different wells after a whole night, at the concentration of 0, 10, 100, 200, 300, 400, 500, 600 nmole. Viability of HeLa cells were tested on a Muse™ Analyser after 24 hours. In every viability measurement, at least 1000 cells were counted.

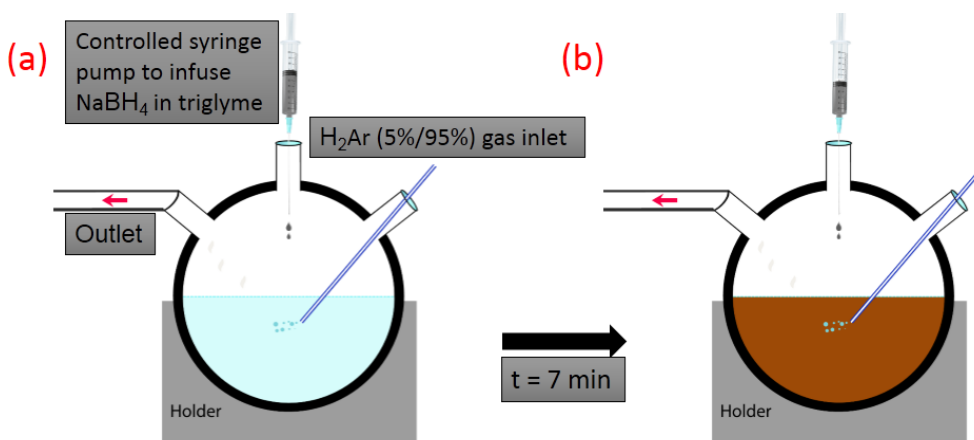
Regarding the long term effect of Ge qdots on live cells viability, HeLa cells were cultivated on a 12-well plate at a density of 15.0×10^3 cells ml⁻¹ well⁻¹. CS₁ was diluted into two concentration solutions of 25 nmole, 250 nmole.

Cell viability was analysed at 24, 48 and 72 hours. Simultaneously, comparison tests were performed with commercial qdots (Qdot 625 ITK Invitrogen A10200: CdSe/ZnS core and shell structure, emission peak at 625 nm). In every viability measurement, at least 1000 cells were counted.

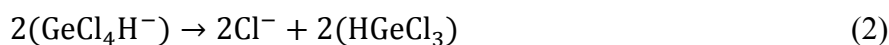
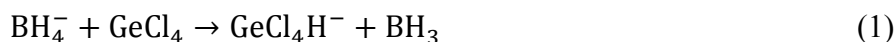
Results and discussion

Scheme 1 demonstrates how the experiment was conducted and a brief formation mechanism of Ge qdots (CS₁) reduced from GeCl₄. CS₁ were prepared by nucleation of Ge atoms liberated by the reduction of GeCl₄²⁷ with a slight modification as designated in the scheme.

A possible formation mechanism of Ge qdots reducing from GeCl₄ is outlined as follows:



Scheme 1. Schematic illustration of formation of luminescent Ge qdots by colloidal synthesis. (a) GeCl₄, PVP and ethylene glycol mixed before infusing NaBH₄ in the triglyme into the solution (see experimental procedure for the details) Here, instead of Ar gas 26, H₂Ar (5%/95%) gas were used to purge the solution in order to prevent possible oxide formation (b) 2 ml of NaBH₄ in the triglyme was added to the solution initially with the rate of 90 ml/min using a syringe pump. Then, the rate was reduced to 9 ml/min for the rest 4 ml of NaBH₄ in the triglyme.



ARTICLE

In the process of the production of Ge qdots by the colloidal synthesis route, the reaction is initiated upon a hydrophilic attack of BH_4^- to GeCl_4 as a source of a hydride ion (Equation 1) which can then lead to the formation of GeCl_3H (Equation 2). Then, the removal of HCl from GeCl_3H (Equation 3) could form reactive germanium(II) species such as GeCl_2 , which could then be inserted into GeH_xCl_y molecular clusters (Equation 4) to act as intermediates in the formation of Ge nanoparticles.

The images of CS_1 immediately after production, and suspended in ethanol, are shown in Figure 1(a). CS_1 , which was then placed onto a quartz boat after being dried by Ar gas, can also be seen in Figure 1(b). The particles are yellow in color.

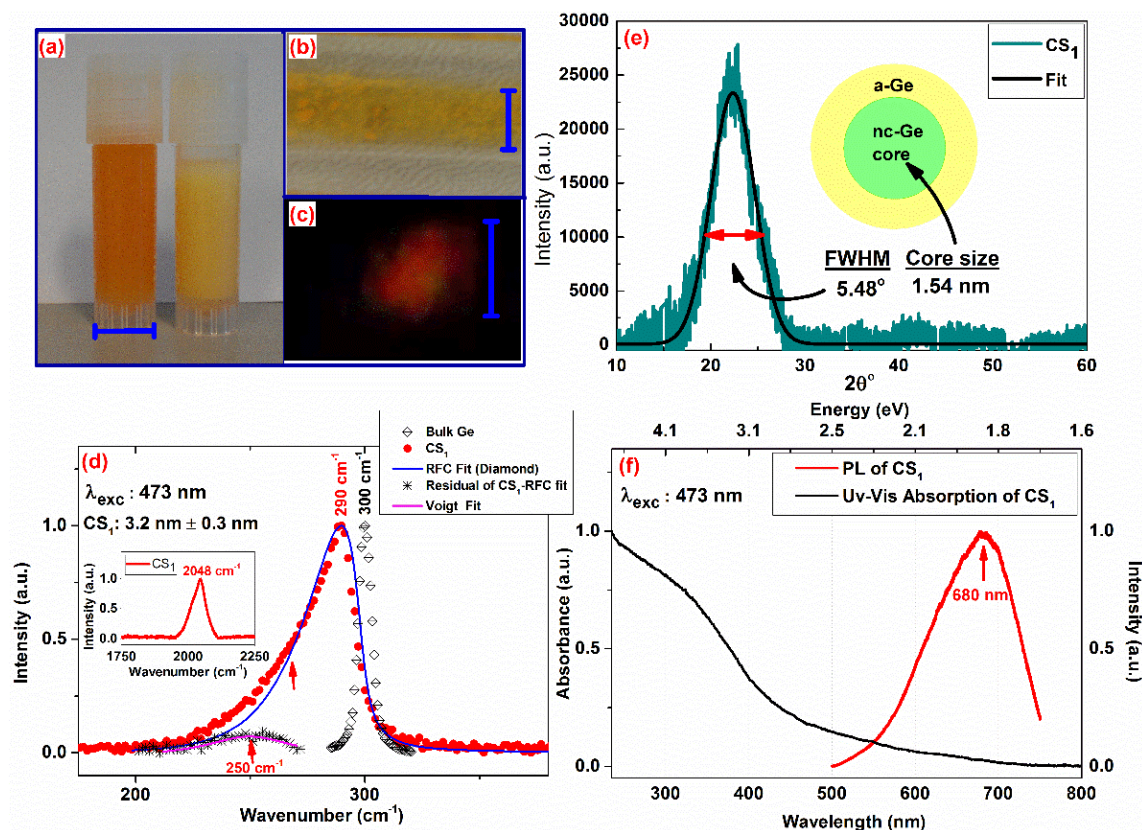


Figure 1 (a) Picture of Ge qdots (CS_1) as-prepared and suspended in ethanol after centrifugation (b) Ge qdots in powder form after dried with Ar gas (c) Luminescent picture of red emitting Ge qdots (the excitation wavelength was 325 nm). Scale bars (all with blue colors) in (a), (b) and (c) are 10 mm, 17 mm and 0.75 mm respectively. (d) Raman shift of CS_1 (red circles) shows an asymmetric Lorentzian peak positioned at 290 cm^{-1} obtained after the RFC fit (blue color). Residual between Raman data of CS_1 and the RFC fit is shown and fitted with a Voigt fit (magenta color) which results in peak position of 250 cm^{-1} . Raman of bulk Ge (black colored diamond) is shown to have a peak position at 300 cm^{-1} . In a-Ge, there is one but a very broad and asymmetric peak ⁶⁵ at 275 cm^{-1} . (See supplementary for Raman of a-Ge reproduced from reference ⁶⁵). The inset in (d) shows stretching mode at 2048 cm^{-1} between Ge and H. For Raman shift and photoluminescent spectroscopy measurements, an excitation wavelength of 473 nm was utilized. (e) X-ray diffraction (XRD) ($\lambda=1.544 \text{ \AA}$, $E=8047 \text{ eV}$) (f) Normalized Uv-Vis absorption spectroscopy and Photoluminescence spectroscopy measurements. The inset core-shell schematic in (e) clarifies the discrepancy between Raman and XRD size calculations such as 3.2 nm and 1.54 nm respectively.

ARTICLE

Raman spectroscopy was used as a first analysis technique to understand the structural properties of CS₁, as well as to estimate the average size of particles. Raman spectroscopy measurements are shown together with the analysis of the data in Figure 1(d). We observed a broad asymmetric peak just below 300 cm⁻¹ as expected for diamond-type Ge qdots²⁰. In addition to the shift in the peak position relative to the bulk Ge optical phonon mode (300 cm⁻¹)⁴³, the Raman spectrum of free-standing CS₁ (see Figure 1(d)) has an asymmetrical Lorentzian-like shape which is an indication that the sample is nanocrystalline^{23,44}. We used the well-known Richter-Fauchet-Campbell (RFC) model^{45,46} based on phonon confinement to estimate the mean size of CS₁ by fitting the corresponding phonon confinement expression to the data. We obtained the particle size to be approximately 3.2 nm for the Raman spectrum given in Figure 1(d). The residual signal between the RFC model and the experimental spectrum is also shown in Figure 1(d). There is a broad peak close to 250 cm⁻¹. Possible origins of this residual might be due to (i) limitation of the phonon confinement model for very small nanoparticles⁴⁷, (ii) amorphous component⁴⁸ or (iii) a metastable phase^{36,49}.

The inset in Figure 1(d) shows a broad peak centered at about 2000 cm⁻¹ that was assigned to the Ge-H stretch mode of CS₁. Hydride termination of Ge nanocrystals using FT-IR studies was reported by several authors with a broad stretching mode between 1900 cm⁻¹ to 2100 cm⁻¹^{50,51, 18,52}. As a complementary technique, EDS data was utilised and shows the traces of Ge (see Figure S5 in supplementary file).

In Figure 2(a), the TEM results are shown for CS₁. The TEM micrograph of CS₁ in Figure 2(a) shows the mean size of CS₁ to be 3.68 nm ± 0.62 nm with a very narrow size distribution from out of 200 qdots of CS₁ in Figure 2(c). Comparison of the size analysis of CS₁ by TEM and the RFC model using Raman spectroscopy results are given in Table S1 (see the supplementary material).

X-ray diffraction (XRD) is frequently used to determine the size and structure of CS₁^[19,20]. Figure 1(e) shows the background subtracted XRD signal for CS₁. The broad peak may suggest a large degree of disorder in samples, but may also be due to the small size of particles. XRD of amorphous Ge (a-Ge) qdots (FWHM=12.68°)²⁷ are found to give a somewhat broader peak compared to the XRD here (5.48°, Figure 1(e)). Using the Scherrer expression²¹, we obtained the size of CS₁ as 1.54 nm. This is to be compared with 3.20 nm and 3.89 nm values extracted from the Raman and TEM respectively. Thus there is a clear discrepancy among TEM, the Raman and XRD results. Given that we do not observe any appreciable number of particles of sizes below 2 nm for CS₁ in TEM (see histogram in Figure 2(b)), this suggests a degree of disorder in our samples, but not as much as in typical a-Ge. One possibility that may explain the result is a core-shell model with a small crystalline core and an amorphous outer layer (see the inset of Figure 1(e)). This would certainly be consistent with the theoretical modelling of small Ge qdots reported previously⁵³.

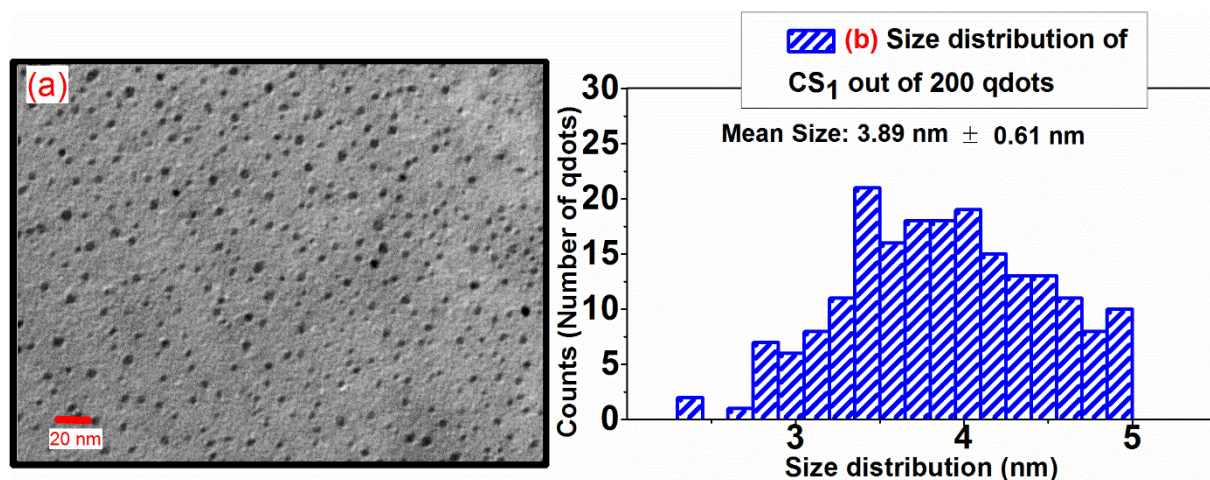


Figure 2 (a) TEM micrograph of CS₁. The graph in (b) is the size distribution of Ge qdots out of 200 qdots. The mean size of Ge qdots was found to be 3.68 nm ± 0.62 nm.

Extended X-ray absorption fine structure (EXAFS) at Ge *K*-edge was used to examine the local environment around Ge atoms and shed light on the possible atomic arrangements. **Figure 3** shows the magnitude of the Fourier transform (MFT) of the k^2 -weighted EXAFS signal, which provides a convenient way to visualize the average local environment around Ge. One can see that only a single peak corresponding to a Ge-Ge bond in the MFT of the EXAFS signal (the first coordination shells at 2.437 ± 0.011 Å for the diamond cubic structure -see the supplementary material for the details of the fit) exists. The presence of only the first coordination shell in the MFT of the EXAFS signal is due to a structural disorder beyond the first coordination shell and the small size. The lack of the Ge-O related signal (at around 1.73 Å) indicates no significant amount of oxides are present in the as-prepared sample. Still, the surface must be terminated and the Ge-H symmetric stretching vibrational mode was observed (as evidence by the Raman data, see inset Figure 1(e)). Clearly, pure H-terminated Ge qdots are unlikely to be colloiddally stable due to the hydrophobic nature of the surface. Therefore, it's quite possible that colloidal stability can be achieved through the bonding of surface hydrogen to other species (e.g. ethoxide as discussed, for example, in other reports⁵⁴).

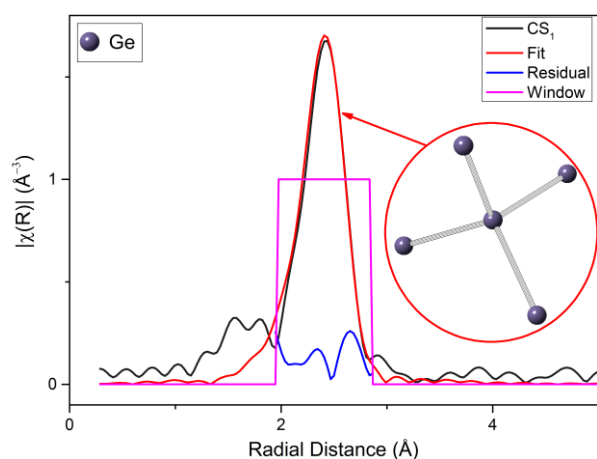


Figure 3 FT modulus of k^2 -weighted EXAFS spectrum of Ge qdots as-prepared (CS_1) at Ge *K*-edge shows only one peak attributed to local disorder and oxide-free surface. The figure also shows the fit, the residual between the fit and the data and the window of the fit. The models of the diamond cubic type of Ge is also demonstrated. The range of the models were chosen between 0-3 Å for the first shells only.

Crystalline bulk Ge has an indirect band-gap that lies within the infrared region of energies ($E_g = 0.67$ eV, 1850 nm)⁵⁵. In order to determine the optical absorption/emission properties of any qdots, such as Ge or CdSe/ZnS, UV-Vis absorption spectroscopy and the PL spectroscopy is widely used^{20,21,28}. Broad UV-Vis absorption spectrum of CS_1 suspended in ultra-pure water is shown in Figure 1(f). The data show that the absorption has a shoulder at ca. 400 nm (3.1 eV). However, the PL peak is found in Figure 1(f) at 680 nm (1.82 eV) suggesting that the nature of emission and absorption events are different. One reason for this could be due to GeH_xCl_y molecular clusters

instead of Ge particles. This would be consistent with the Raman signatures and more importantly explain the presence of the narrow emission spectrum. Moreover, it will yield the stable emission of these molecular clusters in a cell growth environment. It is well-known that the surface contribution to the emission spectra^{19,56-58} may be significant due to the high probability of excitons being captured by the surface states with a subsequent recombination. On the other hand, H-terminated a-Ge⁵⁹ (1.1 eV) was found to have larger band gaps than that of a-Ge⁶⁰ (0.5 eV) or bulk Ge (0.67 eV). Thus, both the large amorphous intermediate region inside the qdot and the surface affect the light emission in CS_1 .

CS_1 synthesized here represents a novel fluorescent product with a potential for bio-applications. Therefore, the biocompatibility and stability of CS_1 for fluorescent imaging was tested on HeLa cells. First, it was necessary to understand the concentrations of Ge qdots that can be suitable for live cell applications. Cell viability as a function of Ge qdot concentration in cell growth medium is shown in Figure 4(a). The results suggest that concentrations below 100 nmole give values of viability close to the qdot free reference. Cell number and viability were found to

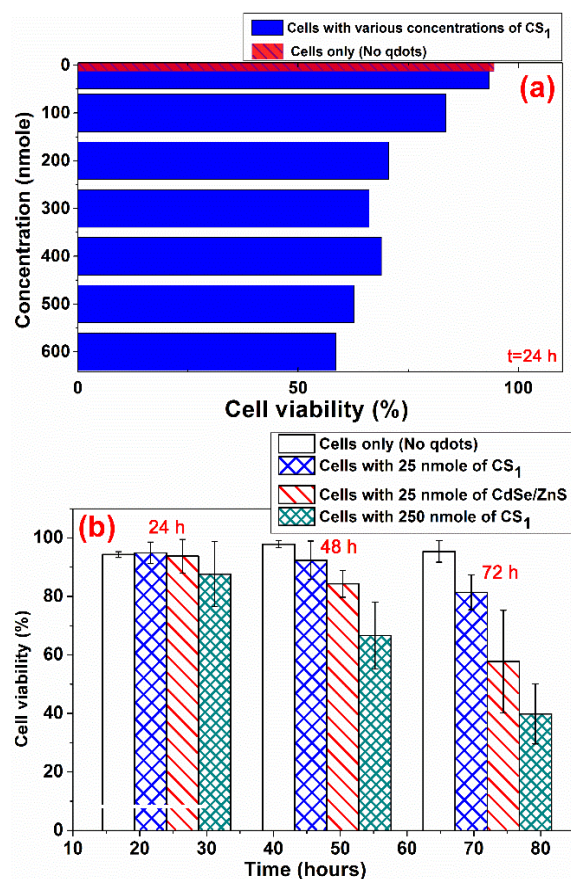


Figure 4 Cell viability of CS_1 when cultured with various concentrations of CS_1 at the end of 24 h is shown in Figure 4(a). Confirmation of the viability test of CS_1 and its comparison with commercial Invitrogen (carboxyl coated CdSe/ZnS) qdots at 25 nmole concentration at different time points show Ge qdots are relatively promising as given in Figure 4(b).

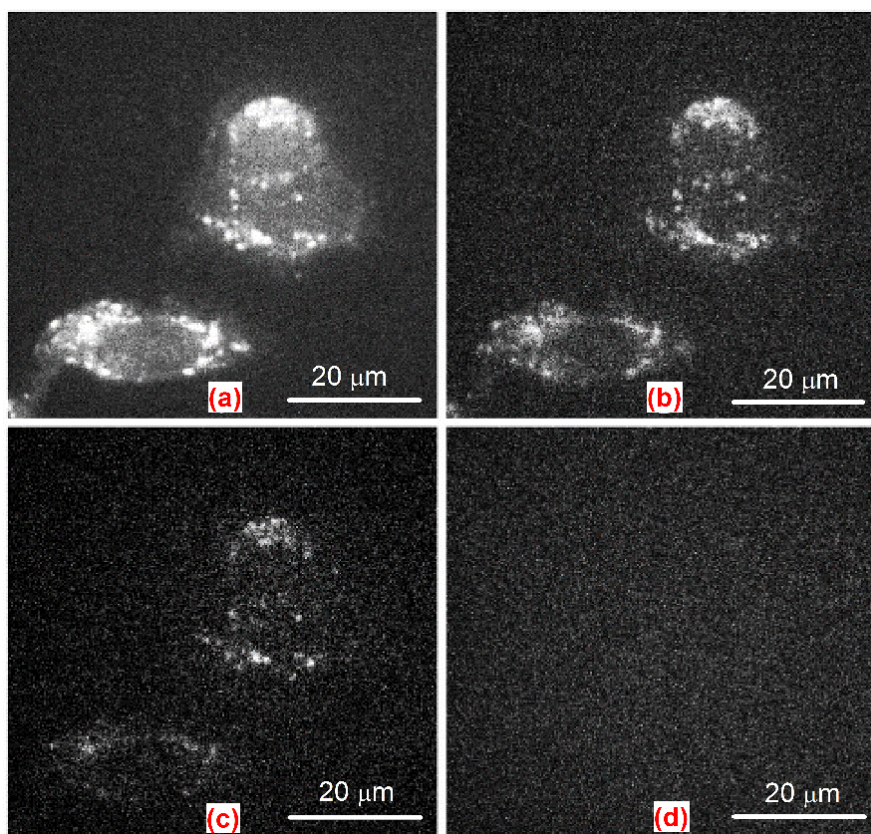


Figure 5 Fluorescence images of CS₁ in Figure 5(a) to 5(d) acquired at various excitation wavelengths; 405, 488, 561, 647 nm shows respectively the range of optical usability. The detected laser power was around 550 nW in the fluorescence images (see also the supplementary material).

depend on Ge qdot concentrations and reduced relatively quickly when seeded with a higher concentration of Ge qdots of 200 nmole (see Figure 4(a)). We further compared the viability of our un-coated as-prepared Ge qdots with commercially available (Invitrogen) carboxyl coated CdSe/ZnS qdots. Figure 4(b) shows the results of the viability tests that were taken over 72 hours and clearly indicates a higher level of biocompatibility of uncoated as-prepared Ge qdots as compared to the commercial carboxyl coated CdSe/ZnS qdots. When using smaller concentrations of the commercial carboxyl coated CdSe/ZnS qdots (e.g. 10 nmole), then the viability results show very little impact on cell viability (see Figure S4 in supplementary part). There are a number of mechanisms⁶¹ reported which are related to CdSe based qdots which might affect their toxicity. Along with the leaking of Cd ions, the CdSe/ZnS qdot degradation, due to an oxide enriched environment, may result in free radicals formation which are understood to contribute to toxicity. Coating CdSe qdots with ZnS helps to decrease Cd ions desorption, although it does not stop the CdSe qdots degradation. In addition to the ZnS coating, commercial carboxyl coated CdSe/ZnS qdots might help slow the CdSe qdot degradation even further. Nevertheless, about 50% of all HeLa cells were killed after 72

hours as shown in Figure 4(b). However, this is not the case for Ge. It has been reported in a wide range of studies^{62,63,64} that Ge can play a therapeutic role by binding free radicals in cells via oxidation. Ge

We tested the CS₁ suitability as a marker for the long term fluorescent imaging of the HeLa cells by using the spinning disk confocal microscopy. The luminescent images from the HeLa cells loaded with CS₁ seem to suggest that the Ge qdots have a higher emission efficiency with the excitation wavelength of 405 nm rather than that of 647 nm, at which there is nearly no emission. This result is consistent with our optical absorption measurement (Figure 2(f)). Based on the fluorescent images in Figure 5, it is clear that CS₁ has reasonably good emission brightness when excited with an appropriate wavelength, despite having relatively lower luminescence efficiency compared to commercial carboxyl coated CdSe/ZnS qdots.

Conclusions

Reflecting upon our collected data, we were able to synthesize colloiddally stable Ge qdots. Combined EXAFS, XRD, Raman and TEM measurements suggest a core-shell structure of Ge qdots with a crystalline core, an amorphous outer layer and a surface with hydrogen-related species. Using Ge qdots, the

luminescent images of HeLa cells were obtained for various excitation wavelengths, which indicate that using Ge qdots as a fluorescence probe is applicable in light microscopy. We tested toxicity of Ge qdots on HeLa cells. The toxicity of Ge qdots and commercial carboxyl coated CdSe/ZnS qdots were investigated using a viability test and from this the Ge qdots were found to be the least toxic of the two. Cells with Ge qdots survived even after 3 days, which suggests that, as well as basic research, the qdots could be used in medical research, clinical imaging and drug screening trials.

Acknowledgements

William R. Little was grateful to The South East Physics Network (SEPnet). Osman Ersoy acknowledges Turkish Ministry of National Education. Helpful discussions with Prof Peter Wyatt from School of Chemistry and Biology, Queen Mary, University of London are gratefully acknowledged.

Notes and references

^a Centre for Condensed Matter and Materials Physics, School of Physics and Astronomy, Queen Mary, University of London, London, E1 4NS, United Kingdom

^b Blizard Institute of Cell and Molecular Sciences, Barts and the Royal London Hospital School of Medicine and Dentistry, Queen Mary, University of London, E1 2AT, United Kingdom.

^c CEMES-CNRS, University of Toulouse, 29 rue Jeanne Marvig, 31055 Toulouse, France.

^d School of Engineering and Materials Science, Queen Mary, University of London, London, E1 4NS, United Kingdom

^e School of Physical Science and Technology, Sichuan University, 29 Wangjiang road, 610064, People's Republic of China

^f Electrical and Electronics Engineering, Bursa Orhangazi University, YILDIRIM Campus, 16310, Yildirim, Bursa, Turkey

Electronic Supplementary Information (ESI) available: [including table of laser power of reflection and incident light for the fluorescence images taken using spinning disk confocal microscopy, the detailed procedure and structural parameters of the EXAFS fit, Raman spectroscopy results and table of size analyses by Raman, TEM and XRD]. See DOI: 10.1039/b000000x/

References

1. P. Alivisatos, *Nat. Biotechnol.*, 2004, **22**, 47–52.
2. T. L. Doane and C. Burda, *Chem. Soc. Rev.*, 2012, **41**, 2885–911.
3. P. Mushonga, M. O. Onani, A. M. Madiehe, and M. Meyer, *J. Nanomater.*, 2012, **2012**, 1–11.
4. U. Resch-genger, M. Grabolle, S. Cavaliere-jaricot, R. Nitschke, and T. Nann, *Nat. Methods*, 2008, **5**, 763–775.
5. B. J. Marcel, M. Mario, P. Gin, W. Shimon, A. A. Paul, and M. Bruchez Jr., *Science (80-)*, 1998, **281**, 2013–2016.
6. J. Fan and P. K. Chu, *Small*, 2010, **6**, 2080–98.
7. T. Pellegrino, S. Kudera, T. Liedl, A. Muñoz Javier, L. Manna, and W. J. Parak, *Small*, 2005, **1**, 48–63.
8. W. Chan and N. Shiao, *Acta Pharmacol. Sin.*, 2008, **29**, 259–66.
9. J. Lovrić, S. J. Cho, F. M. Winnik, and D. Maysinger, *Chem. Biol.*, 2005, **12**, 1227–34.
10. G. Lin, Z. Ding, R. Hu, X. Wang, Q. Chen, X. Zhu, K. Liu, J. Liang, F. Lu, D. Lei, G. Xu, and K.-T. Yong, *RSC Adv.*, 2014, **4**, 5792.
11. J. Liu, F. Erogbogbo, K. Yong, L. Ye, J. Liu, R. Hu, and H. Chen, *ACS Nano*, 2013.
12. S. Hanada, K. Fujioka, Y. Futamura, N. Manabe, A. Hoshino, and K. Yamamoto, *Int. J. Mol. Sci.*, 2013, **14**, 1323–34.
13. L. T. Canham, *Appl. Phys. Lett.*, 1990, **57**, 1046.
14. A. G. Cullis and L. T. Canham, *Nature*, 1991, **353**, 335–338.
15. Y. Maeda, N. Tsukamoto, Y. Yazawa, Y. Kanemitsu, and Y. Masumoto, *Appl. Phys. Lett.*, 1991, **59**, 3168.
16. A. P. Alivisatos, *Science (80-)*, 1996, **271**, 933–937.
17. H. Yang, X. Wang, H. Shi, F. Wang, X. Gu, and X. Yao, *J. Cryst. Growth*, 2002, **236**, 371–375.
18. J. M. Buriak, *Chem. Rev.*, 2002, **102**, 1271–1308.
19. C. Delerue, G. Allan, and M. Lannoo, *J. Lumin.*, 1998, **80**, 65–73.
20. J. R. Heath, J. J. Shiang, and A. P. Alivisatos, *J. Chem. Phys.*, 1994, **101**, 1607–1615.
21. B. R. Taylor, S. M. Kauzlarich, G. R. Delgado, and H. W. H. Lee, *Chem. Mater.*, 1999, **11**, 2493–2500.
22. B. R. Taylor, G. A. Fox, L. J. Hope-Weeks, R. S. Maxwell, S. M. Kauzlarich, and H. W. H. Lee, *Mater. Sci. Eng. B*, 2002, **96**, 90–93.
23. V. Karavanskii, A. Lomov, A. Sutyryn, V. Bushuev, N. Loikho, N. Melnik, T. Zavaritskaya, and S. Bayliss, *Thin Solid Films*, 2003, **437**, 290–296.
24. N. Myung, X. Lu, K. P. Johnston, and A. J. Bard, *Nano Lett.*, 2004, **4**, 183–185.
25. X. Lu, B. A. Korgel, and K. P. Johnston, *Nanotechnology*, 2005, **16**, S389–94.
26. E. J. Henderson, C. M. Hessel, and J. G. C. Veinot, *J. Am. Chem. Society*, 2008, **130**, 3624–3632.
27. N. H. Chou, K. D. Oyler, N. E. Motl, and R. E. Schaak, *Chem. Mater.*, 2009, **21**, 4105–4107.
28. D. D. Vaughn, J. F. Bondi, and R. E. Schaak, *Chem. Mater.*, 2010, **22**, 6103–6108.
29. D. A. Ruddy, J. C. Johnson, E. R. Smith, and N. R. Neale, *ACS Nano*, 2010, **4**, 7459–66.
30. E. Muthuswamy, A. S. Iskandar, M. M. Amador, and S. M. Kauzlarich, *Chem. Mater.*, 2013, **25**, 1416–1422.
31. R. Hardman, *Environ. Health Perspect.*, 2006, **114**, 165–172.
32. S. Sato, S. Nozaki, H. Morisaki, and M. Iwase, *Appl. Phys. Lett.*, 1995, **66**, 3176.
33. S. Nozaki, S. Sato, S. Rath, H. Ono, and H. Morisaki, *Bull. Mater. Sci.*, 1999, **22**, 377–381.
34. S. B. Qadri, E. F. Skelton, and a. W. Webb, *J. Appl. Phys.*, 1983, **54**, 3609.
35. Y. J. Cho, H. S. Im, H. S. Kim, Y. Myung, S. H. Back, Y. R. Lim, C. S. Jung, D. M. Jang, J. Park, E. H. Cha, W. Il Cho, F. Shojaei, and H. S. Kang, *ACS Nano*, 2013, **7**, 9075–84.
36. J. Liu, C. Liang, Z. Tian, S. Zhang, and G. Shao, *Sci. Rep.*, 2013, **3**, 1741.
37. J. Joannopoulos and M. Cohen, *Phys. Rev. B*, 1973, **7**, 2644–2657.
38. T. N. Lambert, N. L. Andrews, H. Gerung, T. J. Boyle, J. M. Oliver, B. S. Wilson, and S. M. Han, *Small*, 2007, **3**, 691–9.
39. S. Prabakar, A. Shiohara, S. Hanada, K. Fujioka, K. Yamamoto, and R. D. Tilley, *Chem. Mater.*, 2010, **22**, 482–486.
40. A. J. Dent, G. Cibin, S. Ramos, a D. Smith, S. M. Scott, L. Varandas, M. R. Pearson, N. a Krumpa, C. P. Jones, and P. E. Robbins, *J. Phys. Conf. Ser.*, 2009, **190**, 012039.
41. B. Ravel and M. Newville, *J. Synchrotron Radiat.*, 2005, **12**, 537–41.
42. S. Zabinsky, J. Rehr, A. Ankudinov, R. Albers, and M. Eller, *Phys. Rev. B*, 1995, **52**, 2995–3009.
43. C. E. Bottani, C. Mantini, P. Milani, M. Manfredini, a. Stella, P. Tognini, P. Cheyssac, and R. Kofman, *Appl. Phys. Lett.*, 1996, **69**, 2409.
44. M. Fujii, S. Hayashi, and K. Yamamoto, *Jpn. J. Appl. Phys.*, 1991, **30**, 687–694.
45. I. H. Campbell and P. M. Fauchet, *Solid State Commun.*, 1986, **58**, 739–741.
46. H. Richter, Z. P. Wang, and L. Ley, *Solid State Commun.*, 1981, **39**, 625–629.
47. V. Paillard, P. Puech, M. a. Laguna, R. Carles, B. Kohn, and F. Huisken, *J. Appl. Phys.*, 1999, **86**, 1921.
48. Y. Sasaki and C. Horie, *Phys. Rev. B*, 1993, **47**, 3811–3818.
49. R. Kobliska, S. Solin, M. Selders, R. Chang, R. Alben, M. Thorpe, and D. Weaire, *Phys. Rev. Lett.*, 1972, **29**, 725–728.
50. C. Su, C.-S. Tsai, C.-E. Lin, K.-H. Chen, J.-K. Wang, and J.-C. Lin, *Surf. Sci.*, 2000, **445**, 139–150.
51. C. Mui, J. H. Han, G. T. Wang, C. B. Musgrave, and S. F. Bent, *J. Am. Chem. Soc.*, 2002, **124**, 4027–4038.

52. F. Maroun, F. Ozanam, and J.-N. Chazalviel, *J. Phys. Chem. B*, 1999, **103**, 5280–5288.
53. L. Pizzagalli, G. Galli, J. Klepeis, and F. Gygi, *Phys. Rev. B*, 2001, **63**, 165324.
54. E. J. Henderson, M. Seino, D. P. Puzzo, and G. A. Ozin, *ACS Nano*, 2010, **4**, 7683–7691.
55. E. Bianco, S. Butler, S. Jiang, O. D. Restrepo, W. Windl, and J. E. Goldberger, *ACS Nano*, 2013, **7**, 4414–21.
56. A. P. Alivisatos, *J. Phys. Chem.*, 1996, **100**, 13226–13239.
57. S. Okamoto and Y. Kanemitsu, *Phys. Rev. B*, 1996, **54**, 16421–16424.
58. J. H. Warner and R. D. Tilley, *Nanotechnology*, 2006, **17**, 3745–3749.
59. I. Chambouleyron, C. F. Graeff, A. R. Zanatta, F. Fajardo, M. Mulato, R. Campomanes, D. Comedi, and F. C. Marques, *Phys. status solidi*, 1995, **192**, 241–251.
60. T. Donovan, W. Spicer, and J. Bennett, *Phys. Rev. Lett.*, 1969, **22**, 1058–1061.
61. T. Jamieson, R. Bakhshi, D. Petrova, R. Pocock, M. Imani, and A. M. Seifalian, *Biomaterials*, 2007, **28**, 4717–32.
62. S. Goodman, *Med. Hypotheses*, 1988, **26**, 207–215.
63. A. Fujii, N. Kuboyama, J. Yamane, S. Nakao, and Y. Furukawa, *Gen. Pharmacol. Vasc. Syst.*, 1993, **24**, 1527–1532.
64. B. Kamen, *A New Approach to Immunity*, Nutrition Encounter, 8th editio., vol. 184.
65. F. Coppari, a. Di Cicco, a. Congeduti, J. C. Chervin, F. Baudalet, and a. Polian, *High Press. Res.*, 2009, **29**, 103–107.